Understanding the atomic-level Green-Kubo stress correlation function for a liquid through phonons in a model crystal

V. A. Levashov

Department of Physics and Astronomy, University of Tennessee, Knoxville, Tennessee 37996, USA

(Received 25 March 2014; revised manuscript received 16 September 2014; published 21 November 2014)

In order to gain insight into the connection between the vibrational dynamics and the *atomic-level* Green-Kubo stress correlation function in liquids, we consider this connection in a model crystal instead. Of course, vibrational dynamics in liquids and crystals are quite different and it is not expected that the results obtained on a model crystal should be valid for liquids. However, these considerations provide a benchmark to which the results of the previous molecular dynamics simulations can be compared. Thus, assuming that vibrations are plane waves, we derive analytical expressions for the atomic-level stress correlation functions in the classical limit and analyze them. These results provide, in particular, a recipe for analysis of the atomic-level stress correlation functions in Fourier space and extraction of the wave-vector and frequency-dependent information. We also evaluate the energies of the atomic-level stresses. The energies obtained are significantly smaller than the energies previously determined in molecular dynamics simulations of several model liquids. This result suggests that the average energies of the atomic-level stresses in liquids and glasses are largely determined by the structural disorder. We discuss this result in the context of equipartition of the atomic-level stress energies. Analysis of the previously published data suggests that it is possible to speak about configurational and vibrational contributions to the average energies of the atomic-level stresses in a glass state. However, this separation in a liquid state is problematic. We also introduce and briefly consider the atomic-level transverse current correlation function. Finally, we address the broadening of the peaks in the pair distribution function with increase of distance. We find that the peaks' broadening (by ≈40%) occurs due to the transverse vibrational modes, while contribution from the longitudinal modes does not change with distance.

DOI: 10.1103/PhysRevB.90.174205 PACS number(s): 46.40.−f, 66.20.Cy, 63.50.Lm

I. INTRODUCTION

In order to understand abrupt increase in viscosity of liquids approaching the glass transition, it is necessary to understand well the nature of viscosity itself. This understanding, however, is still limited [1–11].

Computer simulations have proved to be an important tool in addressing properties of supercooled liquids [1–5]. One standard approach to calculate viscosity in computer simulations is based on the Green-Kubo expression that relates viscosity to the integral of the macroscopic stress-stress correlation function (*sscf*) [1–3,12–16].

Properties of the *sscf* have been extensively studied from *a macroscopic* perspective [1–3,16]. There have been significantly fewer studies that tried to address how the behavior of liquids at the atomic-level translates into the macroscopic behavior of the *sscf* [8–10,17–20].

The situation is similar with a related approach based on considerations of the transverse current correlation function (*tccf*) [1–3,6,7,21–23]. Studies of vibrational dynamics in disordered media with the *tccf* are common and several important results have been obtained with it relatively recently [6,7,21]. However, in all these studies, the *tccf* is treated as a *macroscopic* quantity. Thus the relations between the atomic-level processes and the macroscopic behavior of the *tccf* remain obscure [6,7].

We previously studied the *macroscopic* Green-Kubo *sscf* from a *microscopic* perspective by decomposing it into stress-stress correlation functions (*sscf*s) between the atomic level stresses [8,9]. The approach represents further development of preceding works [16–20]. Obtained data show presence of stress waves in the atomic-level *sscf* and elucidate the connection between the stress waves and viscosity [8,9]. However, it has not been previously discussed *how* stress waves and their properties translate into the observed atomic-level *sscf*. It is difficult to address this issue in liquids, even qualitatively, as vibrational and configurational dynamics in liquids are mixed [24–26]. Moreover, vibrational and configurational dynamics in disordered media are puzzles by themselves [10,21,22,24–36].

On the other hand, as it appears from the literature review, the connection between vibrational dynamics and the *atomic-level sscf* has not been addressed previously even for those systems for which it can be done relatively easily, i.e., for crystals. Applicability of results obtained from crystal models to liquids, in general, is not expected and should be considered with caution. However, it has been demonstrated that parallels between liquid and solid states can be useful [33–36].

Thus, in order to gain at least some qualitative or semi-quantitative insight into the connection between the vibrational dynamics of a model liquid and the atomic-level *sscf* observed in MD simulations [8,9], we examine a crystal-like model in which vibrations are represented by plane waves. These considerations provide the needed insight. The approach also allows developing a basis for analysis in Fourier space of the MD data from a model liquid [8,9]. Discussions of the MD data in this context are presented in Ref. [37]. The considerations in this paper represent further developments and more detailed discussions of some ideas and a model first presented in Ref. [38].

In the context of this paper, it is natural and useful to address several other issues. These issues are of interest and important by themselves.

Thus the atomic-level stress energies have been calculated in the framework of the model. A discussion of these energies, in connection with the previously published MD data [38–41], is presented in Sec. IV.

The *atomic-level tccf* is briefly discussed and it is argued that it is possible to study its behavior in MD simulations in a way that has been applied to the atomic-level *sscf* .

In the framework of the model, it is easy to address the broadening of the peaks in the pair distribution function with increase of distance. This is a known effect observed in x-ray and neutron scattering experiments [42–45]. It follows from the obtained results that the broadening of the peaks (by ≈40%) occurs mostly because of the transverse waves. The changes in the peaks' widths due to the longitudinal waves are significantly smaller.

The paper is organized as follows. In Sec. II, we describe the model. Section III is focused on derivations and analysis of the obtained results. In the end of Sec. III, we also discuss the *tccf* and the broadening of the peaks in the pair distribution function. In Sec. IV, the data from the previous MD simulations are discussed in the context of the results obtained in this paper. The conclusions are given in Sec. V.

II. THE MODEL

We consider a single component system and assume that if the atoms are at equilibrium positions then different atoms have identical environments. It is assumed that every atom interacts harmonically with N_c nearest neighbors. It is also assumed that the distribution of these neighbors is spherically symmetric and that their equilibrium distance from the central atom is a. Finally, we assume that the vibrations in the system are described by plane waves.

A. Continuous spherical approximation

In the following derivations, a summation for every atom n over its nearest neighbors m is often performed. In performing these summations, a continuous spherical approximation is utilized. Thus the summation over m is substituted with the integration over the spherical angles:

$$\sum_m f(\theta_m,\phi_m) \to \frac{N_c}{4\pi}\int f(\theta,\phi)\sin(\theta)d\theta d\phi, \qquad (1)$$

where N_c is the coordination number, which is assumed to be the same for all atoms.

B. Debye's Model

In order to estimate various quantities to which many different waves contribute, it is assumed that different waves contribute independently. The Debye's model is also utilized, i.e., it is assumed that summation over different waves can be changed into the integration over the wave vector q:

$$\frac{dN}{N} = \left(\frac{a}{2\pi}\right)^3 4\pi\, q^2\, dq,\ Q_{\max} = \left(\frac{\pi}{a}\right)\left(\frac{6}{\pi}\right)^{1/3}, \qquad (2)$$

where N is the total number of atoms in the system and also the total number of vibrational states for one polarization. dN is the number of states in the interval dq. $Q_{\max}$ is the maximum value of the wave vector. The equations in (2) are written for one particular polarization of the waves. It will be assumed further, as usual, that there are one longitudinal and two transverse polarizations.

The value of $Q_{\max}$ and the value of the prefactor $[a/(2\pi)]^3$ in (2) are connected by the normalization condition. In principle, different values of $Q_{\max}$ can be assumed for different polarizations of the waves. This issue will not be discussed further.

C. The long-wavelength approximation

In the following, it is assumed sometimes that

$$\sin(\boldsymbol{q}\boldsymbol{a}_{nm}) \approx (\boldsymbol{q}\boldsymbol{a}_{nm}), \quad \cos(\boldsymbol{q}\boldsymbol{a}_{nm}) \approx 1. \qquad (3)$$

Equations (3) are correct if the wavelength of the wave is much larger than the interatomic distance $a \equiv |\boldsymbol{a}_{nm}|$. In the following, the results obtained without the long-wavelength approximation (*lwa*) are derived first and then, for comparison, the results obtained with the *lwa* are presented.

III. DERIVATIONS

The major goal of this section is to derive the expressions for the atomic-level *sscf*s. Another goal is to analyze the Fourier transforms of the shear *sscf*. In the process of derivations of the *sscf*s, the atomic-level stress energies are also calculated. The derivations of the atomic-level stress energies are similar to the derivations of the *sscf*s, but simpler.

The derivations in this section are separated into several steps. At first, expressions for the potential energies of atoms due to different waves, forces on the atoms, and the dispersion relations are calculated. From these expressions, the dependencies of the atomic mean square displacements on temperature are extracted under the assumption of energy equipartition for harmonic vibrations. Then the atomic-level stresses are defined. Further, the expressions for the atomic-level stress energies and stress correlation functions are derived using previously obtained expressions for the mean square displacements. Then the Fourier transforms of the shear-stress correlation function are analyzed.

At the end of the section, we address two separate, but related topics. In particular, we consider the transverse current correlation function and increase in the widths of the peaks in the pair distribution function with increase of distance.

A. Potential energy of an atom due to a plane wave

Let us assume that $\boldsymbol{r}_n^o$ is the equilibrium position of the particle n and $\boldsymbol{u}_n$ is the displacement of the particle n from the equilibrium. Then $\boldsymbol{r}_n = \boldsymbol{r}_n^o + \boldsymbol{u}_n$, $r_{nm} \equiv |\boldsymbol{r}_m - \boldsymbol{r}_n|$, $\boldsymbol{a}_{nm} = a\hat{\boldsymbol{a}}_{nm} \equiv (\boldsymbol{r}_m^o - \boldsymbol{r}_n^o)$, and $\boldsymbol{u}_{nm} = \boldsymbol{u}_m - \boldsymbol{u}_n$. Assuming that the force between the nearest-neighbor atoms n and m at equilibrium positions is zero, in the harmonic approximation, the potential energy of the pair is given by

$$U_{nm} = \frac{k\left(r_{nm} - r_{nm}^o\right)^2}{2} \approx \frac{k}{2}(\hat{\boldsymbol{a}}_{nm}\boldsymbol{u}_{nm})^2. \qquad (4)$$

The solutions for particles' displacements in classical harmonic crystals are plane waves. For a wave with wave

vector $\boldsymbol{q}$,

$$\boldsymbol{u}_n(\boldsymbol{q}) = u_{\boldsymbol{q}}\hat{\boldsymbol{e}}_{\boldsymbol{q}}\,\mathrm{Re}[\chi_n(\boldsymbol{q})], \tag{5}$$

$$\chi_n(\boldsymbol{q}) = \exp[-i(\omega_{\boldsymbol{q}}t - \boldsymbol{q}\boldsymbol{r}_n + \phi_{\boldsymbol{q}})], \tag{6}$$

where $u_{\boldsymbol{q}}$ (real scalar) is the amplitude of the wave, $\hat{\boldsymbol{e}}_{\boldsymbol{q}}$ (real vector) is wave's polarization vector, and $\phi_{\boldsymbol{q}}$ is the phase. In (5), (6), and below, the subscript $\boldsymbol{q}$ shows that parameters with this subscript characterize a particular wave.

From (5) and (6), we get

$$\boldsymbol{u}_{nm}(\boldsymbol{q}) = u_{\boldsymbol{q}}\hat{\boldsymbol{e}}_{\boldsymbol{q}}\mathrm{Re}\{\chi_n(\boldsymbol{q})[\exp(i\boldsymbol{q}\boldsymbol{a}_{nm}) - 1]\}. \tag{7}$$

It is straightforward to show from (4) and (7) that the time average of the potential energy of the atom n due to a particular wave is

$$\langle U_n\rangle_t \approx \left(\frac{1}{2}\right) k u_{\boldsymbol{q}}^2 \sum_m (\hat{\boldsymbol{a}}_{nm}\hat{\boldsymbol{e}}_{\boldsymbol{q}})^2 \sin^2\left(\frac{\boldsymbol{q}\boldsymbol{a}_{nm}}{2}\right), \tag{8}$$

where the factor $1/2$ is introduced to take into account that half of the elastic energy belongs to the atom n, while another half to the atom m.

B. Force on an atom and the dispersion relations

It follows from (4) that the force on the atom n due to its interaction with the atom m is

$$f_{nm}^{\alpha} = -\frac{\partial U_{nm}}{\partial u_n^{\alpha}} = k(\hat{\boldsymbol{a}}_{nm}\boldsymbol{u}_{nm})\hat{a}_{nm}^{\alpha}, \tag{9}$$

where the superscript α labels vector's components. Using the expression (7) for $\boldsymbol{u}_{nm}(\boldsymbol{q})$ in (9) for the total force on the atom n, we get

$$f_n^{\alpha} = \sum_m (k u_{\boldsymbol{q}})(\hat{\boldsymbol{a}}_{nm}\hat{\boldsymbol{e}}_{\boldsymbol{q}})\, a_{nm}^{\alpha}\mathrm{Re}\{\chi_n(\boldsymbol{q})[\exp(i\boldsymbol{q}\boldsymbol{a}_{nm}) - 1]\}. \tag{10}$$

Let us further suppose that we consider crystal lattices with central symmetry. Then for every neighbor m, there is another neighbor m' such that $\boldsymbol{a}_{nm'} = -\boldsymbol{a}_{nm}$. This assumption should be true in the continuous spherical approximation. Taking this into account, we rewrite (10) as

$$f_n^{\alpha} = \sum_m (k u_{\boldsymbol{q}})(\hat{\boldsymbol{a}}_{nm}\hat{\boldsymbol{e}}_{\boldsymbol{q}}) a_{nm}^{\alpha} \times[\cos(\boldsymbol{q}\boldsymbol{a}_{nm}) - 1]\,\cos(\omega_{\boldsymbol{q}}t - \boldsymbol{q}\boldsymbol{r}_n + \phi_{\boldsymbol{q}}). \tag{11}$$

From the fact that plane waves are the solutions for harmonic crystals (5,6,11) and Newton's second law, we get

$$\hat{e}_{\boldsymbol{q}}^{\alpha}\omega_{L,T}^2(\boldsymbol{q}) = \left(\frac{2k}{M}\right)\sum_m (\hat{\boldsymbol{a}}_{nm}\hat{\boldsymbol{e}}_{\boldsymbol{q}})\sin^2\left(\frac{\boldsymbol{q}\boldsymbol{a}_{nm}}{2}\right)a_{nm}^{\alpha}, \tag{12}$$

where M is the particle's mass. Subscripts L and T label longitudinal and transverse polarizations. Multiplication of both sides of (12) on $\hat{e}_{\boldsymbol{q}}^{\alpha}$ and the following summation over α lead to

$$\omega_{L,T}^2(\boldsymbol{q}) = \left(\frac{2k}{M}\right)\sum_m (\hat{\boldsymbol{a}}_{nm}\hat{\boldsymbol{e}}_{\boldsymbol{q}})^2\sin^2\left(\frac{\boldsymbol{q}\boldsymbol{a}_{nm}}{2}\right). \tag{13}$$

The average potential energy of a site due to a wave with the amplitude $u_{\boldsymbol{q}}$ should be equal to $M\omega_{\boldsymbol{q}}^2 u_{\boldsymbol{q}}^2/4$. It is easy to see that multiplication of (13) by $Mu_{\boldsymbol{q}}^2/4$ leads to (8).

In the continuous spherical approximation, (13) should not depend on the direction of $\boldsymbol{q}$ and an analytical expression for (13) can be obtained for the longitudinal and transverse waves. For a longitudinal wave, it is sufficient to assume that $(\boldsymbol{q} \parallel \hat{\boldsymbol{z}})$ and $(\hat{\boldsymbol{e}}_{\boldsymbol{q}} \parallel \hat{\boldsymbol{z}})$. Then $(\hat{\boldsymbol{a}}_{nm}\hat{\boldsymbol{e}}_{\boldsymbol{q}}) = \cos(\theta_{nm})$ and $\sin(\boldsymbol{q}\boldsymbol{a}_{nm}/2) = \sin[(qa/2)\cos(\theta_{nm})]$. For a transverse wave, it is sufficient to assume that $(\boldsymbol{q} \parallel \hat{\boldsymbol{z}})$ and $(\hat{\boldsymbol{e}}_{\boldsymbol{q}} \parallel \hat{\boldsymbol{x}})$. Using (1), we can rewrite (13) as

$$\omega_{L,T}^2(q) = \omega_o^2 D_{L,T}(qa) \equiv \frac{2}{4\pi}\int f_{L,T}(\xi,\theta,\phi)d\Omega, \tag{14}$$

where

$$\omega_o^2 \equiv \left(\frac{k}{M}\right)N_c, \quad \xi \equiv \frac{qa}{2}. \tag{15}$$

For longitudinal (L) and transverse (T) waves,

$$f_L(\xi,\theta,\phi) = \cos^2(\theta)\,\sin^2(\xi\cos(\theta)),$$
$$f_T(\xi,\theta,\phi) = \sin^2(\theta)\cos^2(\phi)\,\sin^2(\xi\cos(\theta)).$$

Integrations of (14) over the spherical angles using the MAPLE(TM) program [46] lead to

$$D_L(qa) = [L_1(\xi) + L_2(\xi)]/(6\xi^3), \tag{16}$$

$$D_T(qa) = [T_1(\xi) + T_2(\xi)]/(12\xi^3), \tag{17}$$

where

$$\begin{aligned} L_1(\xi) &= -6\xi^2\cos(\xi)\,\sin(\xi) + 2\xi^3 - 6\xi\,\cos^2(\xi),\\ L_2(\xi) &= 3\,\cos(\xi)\,\sin(\xi) + 3\xi,\\ T_1(\xi) &= 4\xi^3 + 6\xi\,\cos^2(\xi),\\ T_2(\xi) &= -3\,\cos(\xi)\,\sin(\xi) - 3\xi. \end{aligned} \tag{18}$$

The dependencies of $\sqrt{D_L(qa)}$ and $\sqrt{D_T(qa)}$ on qa, i.e., the dispersion relations, are plotted in Fig. 1.

The dispersion relations for the longitudinal and transverse waves can also be obtained in the *lwa* :

$$\omega_L^{lw}(q) = \left(\frac{\omega_o a}{\sqrt{10}}\right)q, \quad \omega_T^{lw}(q) = \left(\frac{\omega_o a}{\sqrt{30}}\right)q. \tag{19}$$

Thus in the *lwa* , the speeds of the longitudinal waves are $\sqrt{3}$ times larger than the speeds of the transverse waves.

C. Mean square amplitudes of the displacements

If we assume that equipartition holds for our spherical approximation, then the average potential energy of every wave should be equal to $k_bT/2$. Thus we should have

$$\frac{M\omega_{L,T}^2(q)u_{L,T}^2(q)}{4} = \frac{1}{2}\frac{k_bT}{N},$$
$$u_{L,T}^2(q) = 2\left(\frac{k_bT}{kN_c}\right)\left(\frac{1}{D_{L,T}(qa)}\right)\frac{1}{N}, \tag{20}$$

where $u_{L,T}^2(q)$ is the average square amplitude of the longitudinal or transverse waves with the magnitude of the wave

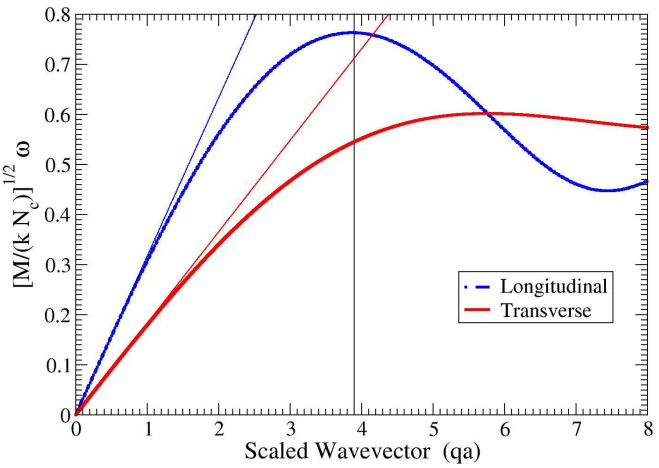

FIG. 1. (Color online) Dispersion curves for the longitudinal and transverse waves in the continuous spherical approximation. Thick lines show the results obtained without the long-wavelength approximation. Thin lines show the results obtained with the long-wavelength approximation. Note that $(Q_{\max}a) \cong 3.9$.

vector q. Thus the squares of the amplitudes are inversely proportional to the dispersion curves shown in the Fig. 1. Note that the wave's amplitudes diverge for small wave vectors. However, according to (2), the volume of the phase space associated with small wave vectors is small and the mean square displacement due to all waves remains finite.

D. Mean square displacements due to all waves

In order to find the mean square displacements due to all waves, assuming that all of them are independent, we have to integrate $\langle u^2_{L,T}(q)\rangle = (1/2)u^2_{L,T}(q)$ of (20) over all q using (2). For the mean square displacements due to all longitudinal waves and both polarizations of all transverse waves, we get

$$\langle u^2_{L,T}\rangle = \left(\frac{k_bT}{kN_c}\right)\gamma_{L,T},$$
$$\gamma_L = 2.8160, \quad \gamma_T = 13.3615. \tag{21}$$

Note that $\langle u^2_T\rangle$ is significantly larger than $\langle u^2_L\rangle$.

It is simpler to evaluate the mean square displacements in the *lwa* . In this case, we get

$$\gamma^{lw}_L = 1.9746, \quad \gamma^{lw}_T = 11.8478. \tag{22}$$

Note that the values of the coefficients in the *lwa* are smaller than without the *lwa* . This is consistent with (20), as the values of the frequencies are always larger in the *lwa* .

E. Atomic-level stress elements

Similarly to the definitions in Refs. [38–40], we define the $\alpha\beta$ component of the local atomic stress element on a particle n as

$$s^{\alpha\beta}_n = \frac{1}{2}\sum_{m\neq n} f^{\alpha}_{nm} r^{\beta}_{nm}, \tag{23}$$

where f^{α}_{nm} is the α component of the force on the particle n caused by the interaction with the particle m and r^{β}_{nm} is the β component of the radius vector from the particle n to the particle m. The sign in (23) is chosen in such a way that an atom under compression has a negative stress/pressure. Using (9), we rewrite (23) as

$$s^{\alpha\beta}_n = \frac{(ka)}{2}\sum_{m\neq n}(\boldsymbol{u}_{nm}\hat{\boldsymbol{a}}_{nm})\hat{a}^{\alpha}_{nm}\hat{a}^{\beta}_{nm}. \tag{24}$$

Then using (7) in (24), we obtain

$$s^{\alpha\beta}_n(\boldsymbol{q}) = \frac{(ka)}{2}u_{\boldsymbol{q}}\chi_n(\boldsymbol{q}) \times \sum_{m\neq n}(\hat{\boldsymbol{e}}_{\boldsymbol{q}}\hat{\boldsymbol{a}}_{nm})[\exp(i\boldsymbol{q}\boldsymbol{a}_{nm}) - 1]\hat{a}^{\alpha}_{nm}\hat{a}^{\beta}_{nm}. \tag{25}$$

Further, like in the transition from (10) to (11), we assume that we consider crystal lattices with central symmetry. For the real part of the stress from (25), we get

$$s^{\alpha\beta}_n(\boldsymbol{q}) = \frac{(kau_{\boldsymbol{q}})}{2}N_c\Upsilon^{\alpha\beta}_1(\boldsymbol{q},\hat{\boldsymbol{e}}_{\boldsymbol{q}})\sin(\omega_{\boldsymbol{q}}t - \boldsymbol{q}\boldsymbol{r}_n + \phi_{\boldsymbol{q}}), \tag{26}$$

where

$$\Upsilon^{\alpha\beta}_1(\boldsymbol{q},\hat{\boldsymbol{e}}_{\boldsymbol{q}}) \equiv \frac{1}{N_c}\sum_{m\neq n}(\hat{\boldsymbol{e}}_{\boldsymbol{q}}\hat{\boldsymbol{a}}_{nm})\sin(\boldsymbol{q}\boldsymbol{a}_{nm})\hat{a}^{\alpha}_{nm}\hat{a}^{\beta}_{nm}. \tag{27}$$

Formulas (26) and (27) express the local atomic stress element through the parameters of the lattice and the parameters of the wave.

F. Atomic-level pressure

In accord with Refs. [38–40], we define the atomic-level pressure as

$$p_n(\boldsymbol{q}) = \frac{1}{3v_o}\left[s^{xx}_n(\boldsymbol{q}) + s^{yy}_n(\boldsymbol{q}) + s^{zz}_n(\boldsymbol{q})\right], \tag{28}$$

where v_o is the atomic volume. Here we assume that the atomic volume is a constant approximately equal to the inverse of the number density, i.e., $v_o \approx 1/\rho_o$.

It follows from (26)–(28) that

$$p_n(\boldsymbol{q}) = \frac{(kau_{\boldsymbol{q}})N_c}{6v_o}\Upsilon^{p}_1(\boldsymbol{q},\hat{\boldsymbol{e}}_{\boldsymbol{q}})\sin(\omega_{\boldsymbol{q}}t - \boldsymbol{q}\boldsymbol{r}_n + \phi_{\boldsymbol{q}}), \tag{29}$$

where

$$\Upsilon^{p}_1(\boldsymbol{q},\hat{\boldsymbol{e}}_{\boldsymbol{q}}) = \frac{1}{N_c}\sum_{m\neq n}(\hat{\boldsymbol{e}}_{\boldsymbol{q}}\hat{\boldsymbol{a}}_{nm})\sin(\boldsymbol{q}\boldsymbol{a}_{nm}). \tag{30}$$

Summation over m (i.e., spherical integration) for a longitudinal wave (note subscript L below) leads to

$$\Upsilon^{p}_{1L}(qa) = \left[\frac{\sin(2\xi) - (2\xi)\cos(2\xi)}{(2\xi)^2}\right], \quad \xi = \frac{qa}{2}. \tag{31}$$

It also follows from (30) that transverse waves do not contribute to the atomic-level pressure.

G. Mean square of the atomic-level pressure

It follows from (29), (30), and (31) that the time averaged square of the atomic-level pressure due to a longitudinal wave

with the wave vector of magnitude q is

$$\langle [p_n(q)]^2 \rangle = \frac{(kau_{\boldsymbol{q}})^2 N_c^2}{72 v_o^2} \Upsilon_{2L}^{p}(qa), \tag{32}$$

where

$$\Upsilon_{2L}^{p}(qa) \equiv \left[\Upsilon_{1L}^{p}(qa)\right]^2. \tag{33}$$

In the *lwa* ,

$$\Upsilon_{2L}^{p,lw}(qa) \approx \tfrac{1}{9}(qa)^2. \tag{34}$$

Use of $u_{\boldsymbol{q}}^2$ from (20) in (32) leads, after integration (2), over q, to

$$\left\langle p_n^2 \right\rangle \approx k_b T \left(\frac{ka^2 N_c}{36 v_o^2}\right) 0.29\ . \tag{35}$$

Calculations in the *lwa* lead to ≈1.11 instead of ≈0.29.

H. Atomic-level pressure energy

In several previous publications, the atomic-level stress energies have been discussed [38–40]. These quantities are of interest, in particular, because of their values in a liquid state. According to MD simulations, the stress energy for every stress component is very close to $(1/4)k_bT = (1/6)(3/2)k_bT$ in the liquid state. It is well known that the average potential energy of a classical 3D harmonic oscillator is equal to $(3/2)k_bT$. Since the stress tensor (24) is symmetric it has six independent components. Thus the values of the atomic-level stress energies are such that it appears that the average potential energy of a 3D harmonic oscillator is equally divided between the six independent components of the atomic-level stress tensor. On this basis, it has been argued in Refs. [38–40] that atoms with the shells of their nearest neighbors can be considered as independent harmonic oscillators. Essentially in Refs. [38–40], the high-temperature limit (i.e., classical limit) of the Einstein model for specific heat has been adopted to describe the behavior of the atomic-level stress energies. In the framework of our model, we essentially consider the classical limit of the Debye model for the atomic-level stress energies.

The expression for the local atomic pressure energy is [38,40]

$$\langle U^p \rangle \equiv \frac{v_o \langle p_n^2 \rangle}{2B}. \tag{36}$$

In order to evaluate (36), we need to know the value of the bulk modulus B. The expressions for the elastic constants have been discussed before [38,40]. The results of their evaluations are

$$B = \frac{\varkappa}{8}, \quad G = \frac{\varkappa}{30}, \quad \varkappa = (ka^2)\frac{N_c}{v_o}, \tag{37}$$

where G is the shear modulus. Using the value of the bulk modulus B for the average pressure stress energy, we get

$$\langle U^p \rangle \approx \left(\frac{1}{4}\right) k_b T \left(\frac{1}{7.76}\right). \tag{38}$$

This energy is approximately 7.76 times smaller than the value of the atomic-level pressure energy that has been obtained in MD simulations of liquids.

In the *lwa* , we get

$$\langle U_{lw}^p \rangle \cong \left(\frac{1}{4}\right) k_b T \frac{1}{2.03}. \tag{39}$$

Thus, in the *lwa* , the atomic-level pressure stress energy is approximately two times smaller than $(1/4)k_bT$, in agreement with Ref. [38]. We discuss atomic-level stress energies further in Sec. IV.

I. Atomic-level shear-stress and shear-stress energy

In accord with Refs. [38–40], we define

$$\sigma_n^{\epsilon}(\boldsymbol{q}, \hat{\boldsymbol{e}}_{\boldsymbol{q}}) \equiv \left(\frac{\sqrt{2}}{v_o}\right) s_n^{xy}(\boldsymbol{q}, \hat{\boldsymbol{e}}_{\boldsymbol{q}}). \tag{40}$$

Both longitudinal and transverse waves contribute to $\sigma_n^{\epsilon}(\boldsymbol{q}, \hat{\boldsymbol{e}}_{\boldsymbol{q}})$. Their contributions depend on the magnitude and direction of $\boldsymbol{q}$ and the direction of $\hat{\boldsymbol{e}}_{\boldsymbol{q}}$. Below, for brevity, we present the formulas for the transverse waves only. The formulas for the longitudinal waves are analogous.

From (26), (27), (40), and (20), we get

$$\left\langle \left[\sigma_{n,T}^{\epsilon}(q)\right]^2 \right\rangle = \left(\frac{A}{4}\right) \frac{2}{N} \left[\frac{\Upsilon_{2T}^{xy}(qa)}{D_T(qa)}\right], \tag{41}$$

where

$$A \equiv k_b T \left(\frac{ka^2 N_c}{v_o^2}\right), \tag{42}$$

$$\Upsilon_{2T}^{xy}(qa) \equiv \left\langle \left[\Upsilon_{1T}^{xy}(\boldsymbol{q}, \hat{\boldsymbol{e}}_{\boldsymbol{q}}, a)\right]^2 \right\rangle, \tag{43}$$

and $\Upsilon_{1T}^{xy}(\boldsymbol{q}, \hat{\boldsymbol{e}}_{\boldsymbol{q}}, a)$ follows from (27). The averaging in (43) and (27) is over all directions of $\hat{\boldsymbol{e}}_{\boldsymbol{q}}$ orthogonal to $\boldsymbol{q}$ and then over the directions of $\boldsymbol{q}$.

We have not been able to produce analytical expressions for $\Upsilon_{2T}^{xy}(qa)$ and $\Upsilon_{2L}^{xy}(qa)$. However, we calculated them numerically [47]. Figure 2 shows the dependencies of

$$H_L^p(qa) \equiv \left[\frac{\Upsilon_{2L}^{p}(qa)}{D_L(qa)}\right](qa)^2, \tag{44}$$

$$H_L^{xy}(qa) \equiv \left[\frac{\Upsilon_{2L}^{xy}(qa)}{D_L(qa)}\right](qa)^2, \tag{45}$$

$$H_T^{xy}(qa) \equiv \left[\frac{\Upsilon_{2T}^{xy}(qa)}{D_T(qa)}\right](qa)^2 \tag{46}$$

on qa without the *lwa* . In (44)–(46), the factor $(qa)^2$ is introduced, as further integration over q is assumed.

We also obtained analytical expressions for (43) in the *lwa* :

$$\frac{\Upsilon_{2L}^{xy,lw}(qa)}{D_L(qa)} \approx \left(\frac{8}{675}\right), \quad \frac{\Upsilon_{2T}^{xy,lw}(qa)}{D_T(qa)} \approx \left(\frac{18}{675}\right). \tag{47}$$

In order to evaluate the mean square stresses due to all waves it is necessary to integrate (41) over q using (2), i.e., to integrate the curves in Fig. 2 over q. The results of these integrations, expressed in terms of the average energy of the atomic-level shear stresses, are

$$\frac{v_o \left\langle \left[\sigma_{n,L,T}^{\epsilon}\right]^2 \right\rangle}{4G} \approx \left(\frac{1}{4}\right) k_b T\ \tau_{L,T}\ , \quad \tau_L \approx \frac{3.1}{135}, \quad \tau_T \approx \frac{20.6}{135}. \tag{48}$$

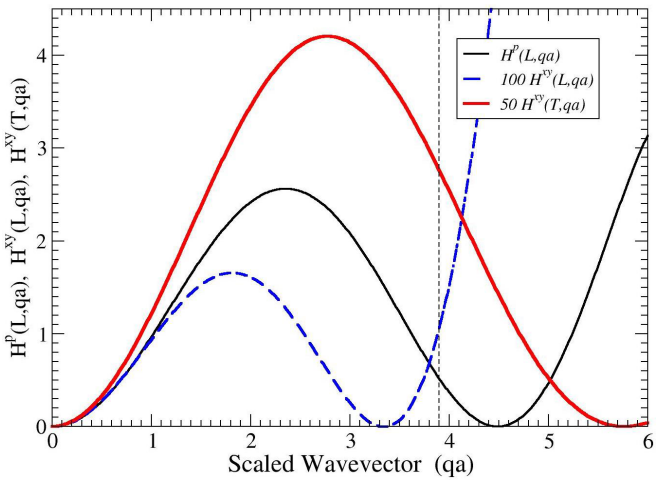

FIG. 2. (Color online) Functions $H_L^p(qa)$, $H_L^{xy}(qa)$, and $H_T^{xy}(qa)$ from (44)–(46). Note that the $H_L^{xy}(qa)$ curve was scaled by 100, while the $H_T^{xy}(qa)$ curve was scaled by 50. Thus the contribution of the transverse waves to the average square of the shear stress is significantly larger than the contribution from the longitudinal waves. Also note that there are two polarizations of the transverse waves, while the figure shows the contribution from one polarization only.

The shear-stress energy coefficient due to all waves is

$$\tau_L + 2\tau_T \approx (44.3/135) \approx \tfrac{1}{3}. \tag{49}$$

This result is three times smaller than the equipartition result, i.e., $(1/4)k_bT$, obtained for liquids in MD simulations in Refs. [39,40]. Also note that this result is more than two times larger than the result that has been obtained for the pressure (38).

In the *lwa* , we get

$$\tau_L^{lw} = \tfrac{24}{135}, \quad \tau_T^{lw} = \tfrac{54}{135}, \tag{50}$$

$$\tau_L^{lw} + 2\tau_T^{lw} = (132/135) \approx 1. \tag{51}$$

Thus in the *lwa* , we essentially have $(1/4)k_bT$ dependence. We discuss atomic-level stress energies further in Sec. IV.

J. Pressure-pressure correlation function

The primary goal of this paper is to address the behavior of the atomic-level stress correlation function, which is analogous to the function $F(t,r)$ which can be derived from the macroscopic Green-Kubo stress correlation function and that has been studied by MD simulations in Refs. [8,9]. Thus we introduce a function which is analogous to $F(t,r)$:

$$C^p(t,r) \equiv \left(\frac{a}{2\pi}\right)^3 N \int_0^{Q_{\max}} C^p(t,r,q)\,4\pi q^2 dq, \tag{52}$$

where

$$C^p(t,r,q) \equiv \langle p_n(t_o,q)\, p_m(t_o+t,q)\rangle. \tag{53}$$

Spherical averaging and the averaging over t_o are assumed in (53).

The correlation function introduced in (52) and (53) is the correlation function per pair of particles. The correlation function between "a central particle" and "the particles in the spherical annulus," introduced in Refs. [8,9] is $4\pi r^2 C^p(t,r)$.

From (29) and (30), it follows that

$$C^p(t,r,q) = \frac{(kau_{\boldsymbol{q}})^2}{36v_o^2}\Upsilon_{2L}^p(qa)\langle \sin(\omega_{\boldsymbol{q}}t_o - \boldsymbol{q}\boldsymbol{r}_n + \phi_{\boldsymbol{q}}) \times \sin[\omega_{\boldsymbol{q}}(t_o+t) - \boldsymbol{q}\boldsymbol{r}_m + \phi_{\boldsymbol{q}}]\rangle. \tag{54}$$

From representing the product of sines as a difference of cosines it follows that one of the cosines gives zero on averaging over $\phi_{\boldsymbol{q}}$. Thus we get

$$C^p(t,r,q) = \frac{(kau_{\boldsymbol{q}})^2}{36v_o^2}\Upsilon_{2L}^p(qa)\frac{1}{2}\left\langle \cos\left(\frac{\omega_{\boldsymbol{q}}t - \boldsymbol{q}\boldsymbol{r}_{nm}}{2}\right)\right\rangle. \tag{55}$$

Further, we rewrite the cosine in (55) as

$$\left\langle \cos\left(\frac{\omega_{\boldsymbol{q}}t}{2}\right)\cos\left(\frac{\boldsymbol{q}\boldsymbol{r}_{nm}}{2}\right)\right\rangle + \left\langle \sin\left(\frac{\omega_{\boldsymbol{q}}t}{2}\right)\sin\left(\frac{\boldsymbol{q}\boldsymbol{r}_{nm}}{2}\right)\right\rangle. \tag{56}$$

Spherical averaging of the second term over the directions of $\boldsymbol{r}_{nm}$ is zero. Spherical averaging in the first term gives

$$\left\langle \cos\left(\frac{\boldsymbol{q}\boldsymbol{r}_{nm}}{2}\right)\right\rangle = 2\frac{\sin(qr/2)}{(qr/2)}. \tag{57}$$

Using the expression (20) for $u_{\boldsymbol{q}}^2$, we rewrite (55) as

$$C^p(t,r,q) = \left(\frac{A}{36}\right)\frac{2}{N}\left[\frac{\Upsilon_{2L}^p(qa)}{D_L(qa)}\right] \times \left[\frac{\cos(\omega_{\boldsymbol{q}}t/2)\sin(qr/2)}{(qr/2)}\right], \tag{58}$$

where A is given by (42) and, according to (14), $\omega_{\boldsymbol{q}} = \omega_o\sqrt{D_L(qa)}$. The product of the cosine and sine in (58) can be rewritten as

$$\frac{1}{2}\left[\sin\left(\frac{qr - \omega_{\boldsymbol{q}}t}{2}\right) + \sin\left(\frac{qr + \omega_{\boldsymbol{q}}t}{2}\right)\right]. \tag{59}$$

The first sine in (59) corresponds to a wave propagating away from the central particle. This sine is zero when $r - (\omega_{\boldsymbol{q}}/q)t = 0$. Thus the speed of this wave, for a given r, should be determined from the time when the sign of the sine changes from positive to negative.

The argument of the second sine in (59) is always positive for $t > 0$ and $r > 0$. For $t > 0$, the contribution to the *sscf* due to all waves from the second sine is much smaller than from the first sine.

In order to find the pressure correlation function due to all waves it is necessary to integrate (58) over all q using (2). Figure 3 shows the results for the pressure-pressure correlation function due to all waves without the *lwa* . Figure 4 shows the result with the *lwa* .

K. Shear-stress correlation function

In order to introduce the shear-stress correlation function, which is analogous to the function $F(t,r)$ in Refs. [8,9], we introduce at first a correlation function due to a particular

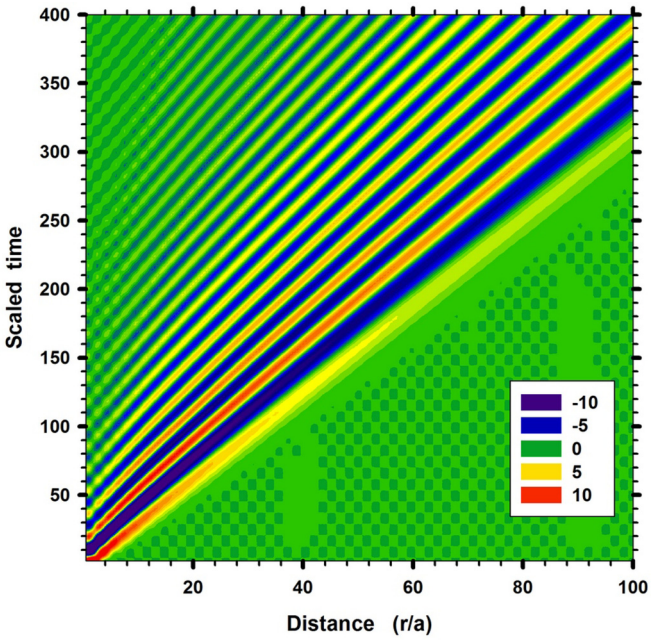

FIG. 3. (Color online) Pressure-pressure correlation function without the long-wavelength approximation. The scaled time is $\omega_o t$.

transverse wave:

$$C^{\epsilon}_{T,\boldsymbol{q}}(t,r,\boldsymbol{q},\hat{\boldsymbol{e}}_{\boldsymbol{q}}) \equiv \left(\frac{2}{v_o^2}\right)\left\langle s_n^{xy}(t_o,\boldsymbol{q},\hat{\boldsymbol{e}}_{\boldsymbol{q}}) s_m^{xy}(t_o+t,\boldsymbol{q},\hat{\boldsymbol{e}}_{\boldsymbol{q}})\right\rangle$$
$$= \left(\frac{A}{4}\right)\frac{2}{N}\left[\frac{\Upsilon_{2T}^{xy}(\boldsymbol{q},\hat{\boldsymbol{e}}_{\boldsymbol{q}},a)}{D_T(qa)}\right]$$
$$\times\langle \sin[\omega_{\boldsymbol{q}} t_o - \boldsymbol{q}\boldsymbol{r}_n + \phi_{\boldsymbol{q}}]\sin[\omega_{\boldsymbol{q}}(t_o+t)$$
$$-\boldsymbol{q}\boldsymbol{r}_m + \phi_{\boldsymbol{q}}]\rangle\ . \qquad (60)$$

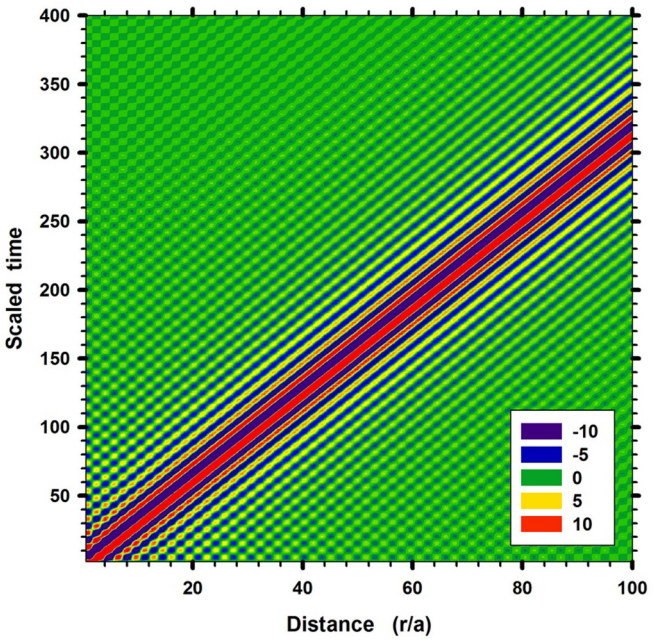

FIG. 4. (Color online) Pressure-pressure correlation function with the long-wavelength approximation. The scaled time is $\omega_o t$.

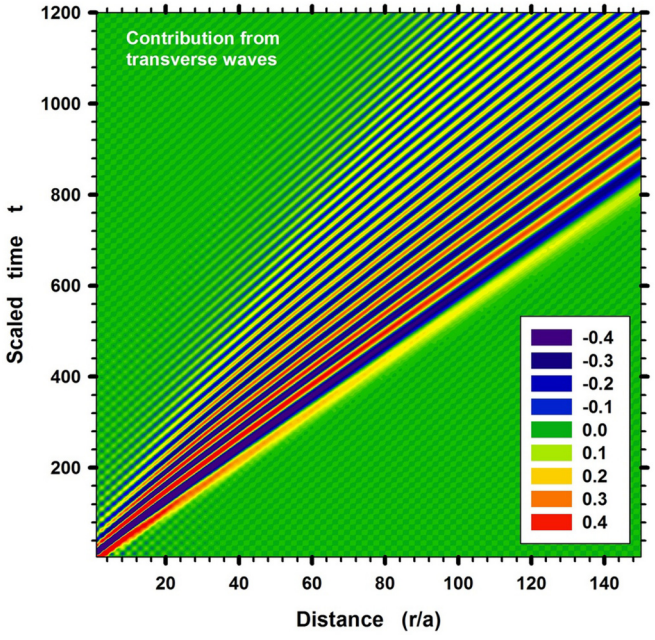

FIG. 5. (Color online) Contribution from one polarization of the transverse waves to the shear-stress correlation function. The scaled time is $\omega_o t$. No damping of the waves is assumed.

In (60), A is given by (42). Similarly to how it has been done in the transition from (55) to (58) for the pressure-pressure correlation function, the averaging over the directions of $\boldsymbol{r}_{nm}$ is performed first. Then the averagings over the polarization and the direction of the wave are performed. These averagings are identical to the averagings done in the derivations of (41,43). Thus we get

$$C^{\epsilon}_T(t,r) = \left(\frac{a}{2\pi}\right)^3 N\int_0^{Q_{\max}} C^{\epsilon}_T(t,r,q)\,4\pi q^2 dq, \qquad (61)$$

where

$$C^{\epsilon}_T(t,r,q) = A\frac{2}{N}\left[\frac{\Upsilon_{2T}^{xy}(qa)}{D_T(qa)}\right]$$
$$\times\left[\frac{\cos(\omega_{\boldsymbol{q}} t/2)\sin(qr/2)}{(qr/2)}\right]. \qquad (62)$$

Figure 5 shows the *sscf* calculated numerically from (61,62) with the coefficient $A = 1$.

Formulas (61) and (62) have been derived under the assumption that vibrations are nondecaying plane waves. In order to make a comparison with a liquid state, it is reasonable to assume that the vibrations decay with the increase of time. In order to study how this attenuation can affect the *sscf*, we phenomenologically introduce into (62) a damping function. Thus we define

$$C^{\epsilon,\mathrm{damp}}_T(t,r,q) \equiv C^{\epsilon}_T(t,r,q)E(\omega_{\boldsymbol{q}},t), \qquad (63)$$

where

$$E(\omega_{\boldsymbol{q}},t) = \exp[-0.3(\omega_{\boldsymbol{q}}/\omega_o)^2\omega_o t]. \qquad (64)$$

The form of the damping function (64) is based on multiple studies on attenuation of waves in liquids [22,48].

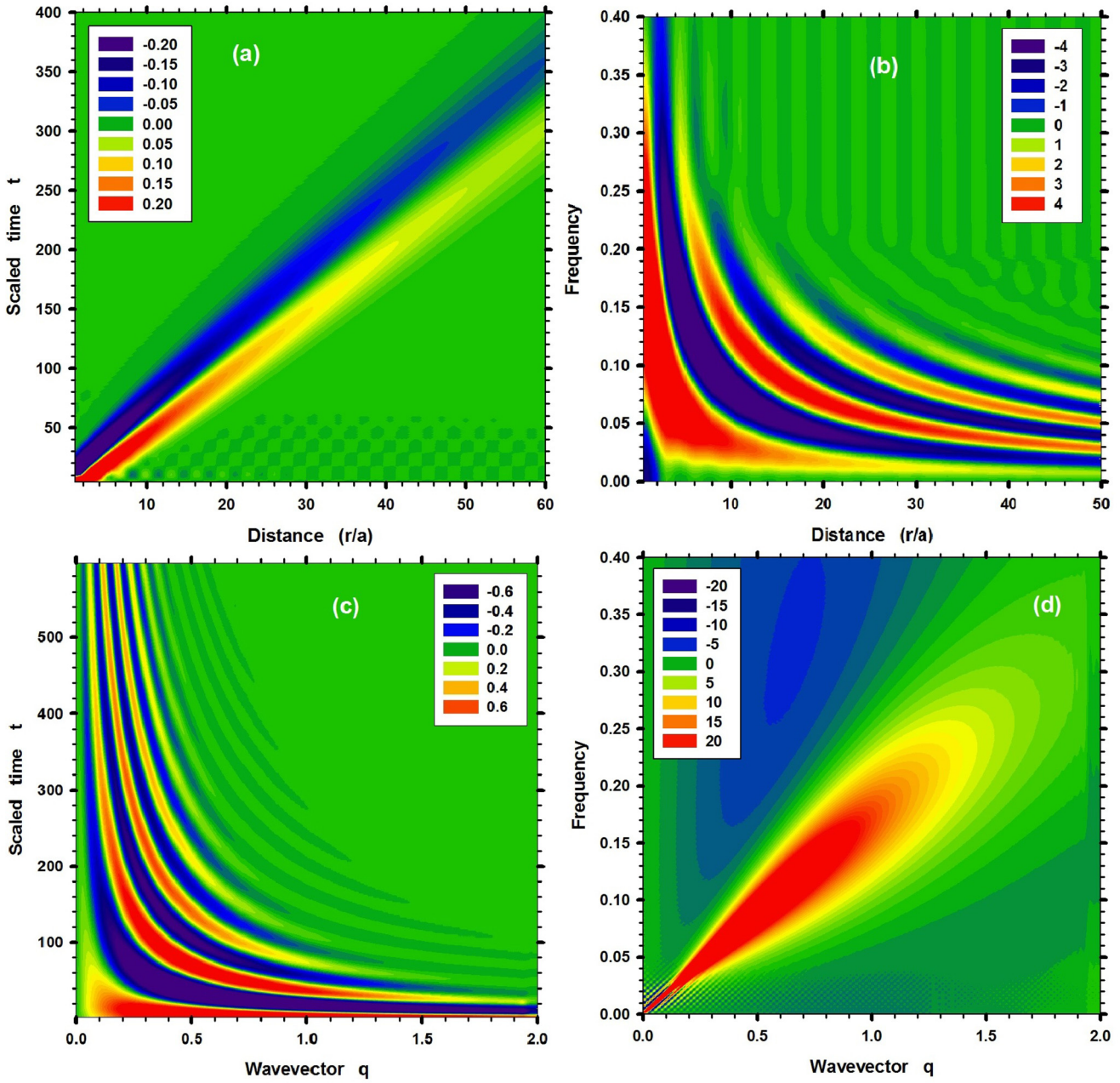

FIG. 6. (Color online) Scaled shear-stress correlation function, $f(t,r)$ (66), due to the transverse waves with exponential damping in time and its Fourier transforms. (a) r-scaled shear-stress correlation function (62,66) integrated over all q with $E(\omega_q,t)$ given by (64). It was assumed that the numerical prefactor is equal to 1. Scaled time is $\omega_o t$. (b) Time to frequency Fourier transform of the scaled stress correlation function in the panel (a). Angular frequency is measured in units of ω_o. (c) Distance to wave vector Fourier transform of the scaled stress correlation function in the panel (a). The unit of the wave vector is $1/a$. (d) Time to frequency and distance to wave-vector Fourier transforms of the scaled stress correlation function in the panel (a). Note that the center of the diagonal high-intensity region follows the dispersion curve for the transverse waves in Fig. 1. It is clear that the broadening of the dispersion curve is caused by the exponential damping (64).

Panel (a) of Fig. 6 shows the *sscf* calculated from (61,63), i.e., now with $C_T^{\epsilon,\mathrm{damp}}(t,r,q)$ instead of $C_T^{\epsilon}(t,r,q)$.

It is of interest to compare the panel (a) of Fig. 6 with the panel (b) of Fig. 4 in Ref. [9]. Note that in the present paper we changed the axes and now the x axis shows the distance, while the y axis shows the time. In the panel (b) of Fig. 4 in Ref. [9], we see two waves. One wave is longitudinal and another wave is transverse. There is also the structural contribution to the *sscf*. In the panel (a) of Fig. 6, we see the contribution from the transverse waves only, as the contribution from the longitudinal waves has not been included. The structural contribution is also absent in the panel (a) of Fig. 6. Besides the differences mentioned above, it is clear that the contribution to the *sscf* from the transverse waves observed in MD simulation is qualitatively similar to the *sscf* obtained from the formulas in this section if the damping (64) is included. In particular, if we consider how the intensity changes with the increase of time for a given distance, we observe at first positive intensity

and then negative intensity. This observation is natural in view of the paragraph after (59).

Formula (59) suggests that the speed of the wave corresponds to the slope of the boundary between the positive and negative intensities. This interpretation is different from the one adopted in Ref. [9]. There, it was assumed that the wave's speed should be extracted from the maximum of the positive intensity. With the new interpretation, the speed of the longitudinal waves in the panel (b) of Fig. 4 in Ref. [9] is $c_l \approx 7500$ m/s. It was previously argued that it is 6000 m/s. The new speed of the transverse waves is $c_t \approx 5000$ m/s, while before it was argued that it is 3000 m/s. Note that, according to the new values, $c_l/c_t \approx 1.5$. This value is close to $\sqrt{3}$ predicted by Eq. (19).

L. Fourier transforms of the shear-stress correlation function

The atomic-level *sscf*s, like those in (58) and (62), can be calculated in MD simulations [8,9]. In this section we analyze what information can be obtained by performing the Fourier transforms of these *sscf*s [(58) and (62)]. Thus, further, we consider a function that is structurally similar to the *sscf*s [(58) and (62)]:

$$f(t,r) \equiv \int_0^{Q_{\max}} h(q,t) \cos\left(\frac{\omega_{\boldsymbol{q}} t}{2}\right) \sin\left(\frac{qr}{2}\right) dq. \quad (65)$$

For the shear *sscf* due to the transverse waves [(61) and (63)] with damping [(63) and (64)], for example, we have

$$f(t,r) \equiv r C_T^{\epsilon,\mathrm{damp}}(t,r), \quad (66)$$

$$h(q,t) \equiv \alpha \left(\frac{Y_{2T}^{xy}(q)}{D_T(qa)}\right) E(\omega_{\boldsymbol{q}},t)\, q, \quad (67)$$

where α is a numerical coefficient and $E(\omega_{\boldsymbol{q}},t)$ is given by (64). Note that the case without damping is obtained from (67) by assuming that $E(\omega_{\boldsymbol{q}},t) = 1$. Also note that $f(t,r)$, as we define it, is the correlation function per pair of particles multiplied by r.

Further we define

$$\tilde{f}(t,q) \equiv \int_0^{\infty} f(t,r)\, \sin(qr) dr, \quad (68)$$

$$\tilde{f}(\omega,r) \equiv \int_0^{\infty} f(t,r)\, \cos(\omega t) dt, \quad (69)$$

$$\tilde{f}(\omega,q) \equiv \int_0^{\infty}\int_0^{\infty} f(t,r)\, \cos(\omega t)\, \sin(qr)\, dt\, dr. \quad (70)$$

From (68), (65), and (67), we get

$$\tilde{f}(t,q) \equiv \left(\frac{\pi}{2}\right) h(2q,t) \cos\left(\frac{\omega_{2q} t}{2}\right), \quad (71)$$

where $\omega_{2q}^2 = \omega_o^2 D_T(2qa)$. Thus $\tilde{f}(t,q)$, for every value of q, oscillates in time with the period determined by the dispersion relation. The decrease in the amplitude of oscillations with increase of time is determined by the damping function $E(\omega_{\boldsymbol{q}},t)$ (67). If there is no damping function, the amplitude of oscillations remains constant.

The situation with the Fourier transform of $f(t,r)$ over time, if the damping is present, is more complicated. If there is no damping, i.e., if $E(\omega_{\boldsymbol{q}},t) = 1$, then from (69), (65), and (67), the Fourier transform of $f(t,r)$ over t is

$$\tilde{f}(\omega,r) \equiv \left(\frac{\pi}{2}\right) h(q_{2\omega}) \sin\left(\frac{q_{2\omega} r}{2}\right), \quad (72)$$

where $(2\omega)^2 = \omega_o^2 D_T(q_{2\omega} a)$. Thus, in the absence of damping, the Fourier transform of $f(t,r)$ over time (72) should exhibit for every frequency constant amplitude oscillations with the wavelength determined by the dispersion relation.

In the absence of damping, the Fourier transforms of $f(t,r)$ over r and t (70) lead to

$$\tilde{f}(\omega,q) \equiv \left(\frac{\pi}{2}\right)^2 h(2q) \delta\left(\omega - \frac{\omega_{2q}}{2}\right), \quad (73)$$

i.e., to the dispersion relation.

The function $\tilde{f}(\omega,q)$ can be obtained by the Fourier transform over time of the expression (71). It is clear from the form of (71) that the presence of damping in $h(2q,t)$ should lead to the broadening of the δ function in (73).

Panel (a) of Fig. 6 shows the function $f(t,r)$ from (65)–(67) with $E(\omega_{\boldsymbol{q}},t)$ given by (64). It was assumed that $\alpha = 1$. Panels (c), (b), and (d) show the Fourier transforms (68)–(70) of the function $f(t,r)$.

M. Transverse current correlation function

The transverse current correlation function (*tccf*) is often used in studies of liquid dynamics [1–3,6,21–23]. However, usually it is considered as a *macroscopic* quantity. In this section, we suggest that the *tccf* also can be studied from a *microscopic* perspective, as it has been done with the *sscf* [8,9].

In agreement with the definitions in Refs. [1–3,6,21–23], we consider the following expression for the real part of the transverse current:

$$J_T(\boldsymbol{k},t) = \sum_i \boldsymbol{v}_i^T(t)\, \cos[\boldsymbol{k}\boldsymbol{r}_i(t)], \quad (74)$$

where $\boldsymbol{v}_i^T(t) = \boldsymbol{v}_i(t) - (\boldsymbol{v}_i(t)\hat{\boldsymbol{k}})$. For the contribution from a transverse wave with the wave vector $\boldsymbol{q}$ and the polarization $\hat{\boldsymbol{e}}_{\boldsymbol{q}}$ from (74), (5), and (6), we get

$$\begin{aligned} J_T(\boldsymbol{k},\boldsymbol{q},\hat{\boldsymbol{e}}_{\boldsymbol{q}},t) &= -u_{\boldsymbol{q}} \hat{\boldsymbol{e}}_{\boldsymbol{q}} \omega_{\boldsymbol{q}} B_1(\boldsymbol{k},\boldsymbol{q},t), \\ B_1(\boldsymbol{k},\boldsymbol{q}) &\equiv \sum_i \sin[\omega_{\boldsymbol{q}} t - \boldsymbol{q}\boldsymbol{r}_i(t) + \phi_{\boldsymbol{q}}] \cos[\boldsymbol{k}\boldsymbol{r}_i(t)]. \end{aligned} \quad (75)$$

Then for the correlation function due to this wave, we have

$$C_{JT}(\boldsymbol{k},\boldsymbol{q},\hat{\boldsymbol{e}}_{\boldsymbol{q}},t) \equiv \frac{1}{N} \langle J_T(\ldots,t_o) J_T(\ldots,t_o+t) \rangle. \quad (76)$$

The averaging in (76) is over the initial time t_o.

From (75), (76), and (20), using the same logic that has been used in the derivations of (58) and (62), we get

$$C_{JT}(\boldsymbol{k},\boldsymbol{q},\hat{\boldsymbol{e}}_{\boldsymbol{q}},t) = \left(\frac{C_e}{N}\right) \cos(\omega_{\boldsymbol{q}} t)(X_1 + X_2), \quad (77)$$

$$C_e \equiv \frac{u_{\boldsymbol{q}}^2 \omega_{\boldsymbol{q}}^2}{4} = \frac{k_b T}{2NM}, \quad X_{1,2} \equiv \sum_{ij} \frac{\sin(|\boldsymbol{k} \pm \boldsymbol{q}| r_{ij})}{|\boldsymbol{k} - \boldsymbol{q}| r_{ij}}. \quad (78)$$

In the derivations of (77) and (78), there also appear two other terms, which, however, vanish in the limit $N \to \infty$. After the integration over $\boldsymbol{q}$, the contributions from X_1 and X_2 terms are equal to each other. Note that if $\boldsymbol{k} = 0$ then the structure of (77) and (78) is similar to the structures of (58) and (62). It follows from (75)–(78) that it is possible to introduce and consider the *atomic-level tccf* similarly to how it has been done for the atomic-level *sscf* in Refs. [8,9].

N. The widths of the peaks in the pair distribution function

Atoms located close to each other in crystal lattices exhibit a certain degree of coherence in their motions. Because of this coherence, the peaks in the pair distribution function at small distances are narrower than at large distances [42–45]. The dependence of the peaks' widths on distance has been investigated previously using a detailed model and evolved simulations [43,44]. In the framework of our model, we can address this effect in a simple and intuitive way.

The average square of the peak width in the pair distribution function is determined by [43,44]

$$\langle(\Delta r_{nm})^2\rangle \cong \left\langle\left(\hat{\boldsymbol{r}}^o_{nm}\boldsymbol{u}_{nm}\right)^2\right\rangle. \tag{79}$$

In (79), the notation $\langle\ldots\rangle$ is used for the time and spherical averagings. Spherical averaging in (79) is over the directions of $\boldsymbol{r}^o_{nm}$, i.e., over the positions of the atoms m. The expression for $\langle(\Delta r_{nm})^2\rangle$ is analogous to the expression (4), but with $\boldsymbol{r}^o_{nm}$ instead of $\boldsymbol{a}_{nm}$. Thus, in analogy with how (8) has been derived, we obtain

$$\langle(\Delta r_{nm}(\boldsymbol{q}))^2\rangle \cong u^2_{\boldsymbol{q}}\left\langle\left(\hat{\boldsymbol{r}}^o_{nm}\hat{\boldsymbol{e}}_{\boldsymbol{q}}\right)^2\sin^2\left(\frac{\boldsymbol{q}\boldsymbol{r}^o_{nm}}{2}\right)\right\rangle. \tag{80}$$

Using the expression (20) for $u^2_{\boldsymbol{q}}$, we get

$$\frac{N_c k\langle(\Delta r_{nm}(\boldsymbol{q}))^2\rangle}{2k_bT} \cong \frac{\left\langle\left(\hat{\boldsymbol{r}}^o_{nm}\hat{\boldsymbol{e}}_{\boldsymbol{q}}\right)^2\sin^2\left(\frac{\boldsymbol{q}\boldsymbol{r}^o_{nm}}{2}\right)\right\rangle}{\sum_m(\hat{\boldsymbol{a}}_{nm}\hat{\boldsymbol{e}}_{\boldsymbol{q}})^2\sin^2\left(\frac{\boldsymbol{q}\boldsymbol{a}_{nm}}{2}\right)}. \tag{81}$$

In order to estimate the peak width due to all waves, it is necessary to integrate the numerator and denominator on the right-hand side of (81) over the spherical angles and then their ratio over all q using (2). The dependencies of the peak's width on the absolute value of r^o_{nm} (assuming that $N_c = 1$) for all longitudinal waves and one polarization of all transverse waves are shown in Fig. 7.

For large r^o_{nm}, motions of the atoms n and m should be uncorrelated. It is straightforward to show from (79) that if atoms n and m vibrate independently then $\langle(\Delta r_{nm})^2\rangle = (2/3)\langle(u_n)^2\rangle$. This should be the large r^o_{nm} limit of the peak's width. In order to get this limit from the curves in Fig. 7 it is necessary to multiply the limiting value by 2 for the longitudinal waves (the prefactor in (81)) and by 4 for the transverse waves (the prefactor and two polarizations). Then the results can be compared with (21).

Note that the contribution to the peak's width from the shear waves increases more than twice as the distance increases from the nearest neighbors, i.e., $(r/a) = 1$ to infinity. Also note that there is essentially no change in the peak's width with distance due to the longitudinal waves.

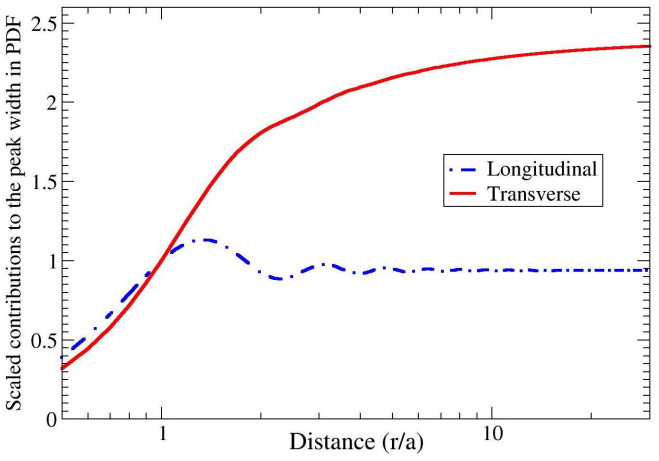

FIG. 7. (Color online) Contributions to the peak's width in the pair distribution function from longitudinal and transverse waves as a function of distance. The blue curve represents contributions from all longitudinal waves. The red curve represents contributions from one polarization of all transverse waves.

IV. DISCUSSION OF THE ATOMIC-LEVEL STRESS ENERGIES

In this section, we discuss why the atomic-level stress energies obtained in MD simulations are significantly larger than the values obtained within the model considered in this paper. The results of the previous MD simulations on a model iron (see Fig. 3 of Ref. [39] and Fig. 5 of Ref. [40]) can be summarized as follows. In the glass state ($T < 900$ K), the stress energy of every independent component of the atomic-level stress tensor depends on the temperature approximately as $U_o + (1/10)k_bT$ [39,40]. Thus, in the glass state at $T = 0$ K, the average energy of every atomic-level stress component has a finite value, U_o. The value of U_o depends on cooling history, but approximately $(U_o/k_b) \approx 200$ (K). In the liquid state ($T > 1300$ K), the energy of every component of the atomic-level stress tensor is equal to $(1/4)k_bT$ with rather good precision. It has been observed in MD simulations that different components of the atomic-level stress tensor have equal values of the stress energies. Thus it is possible to speak about the equipartition of the total atomic-level stress energy between the six independent stress components.

The $(1/4)k_bT$ temperature dependence of the atomic-level stress energies has been analytically derived from the Boltzmann distribution for the atomic-level stress energies in a model that assumes that the atoms with their nearest-neighbor shells act as independent 3D harmonic oscillators [38,40]. In this model, the definition of the atomic-level stresses automatically includes into itself variations in the coordination numbers between the different atoms. Because of this definition, the coordination number N_c is not explicitly present in the derivations.

The derivation of the $(1/4)k_bT$ temperature dependence implies the presence of ergodicity for every central atom and its coordination shell. In the liquid state, time averaging over every atom is equal to the ensemble averaging. In the glass state, the coordination numbers of many atoms are fixed on the time scale of a simulation. Thus time averaging

of the stress energy for every particular atom is not equal to the ensemble averaging. Therefore different temperature dependencies of the atomic-level stress energies in the glass and liquid states might reflect the breakdown of ergodicity at the glass transition.

At $T = 0$ K, there are no vibrations in the classical systems. Thus, in the glass state, the value of the atomic-level stress energies at $T = 0$ K, i.e., U_o, is determined only by the structural disorder, which also includes variations in the coordination numbers between the different atoms, as can be seen in Fig. 2 of Ref. [41]. In the glass state, it is natural to associate U_o with the structural contribution, while $(1/10)k_bT$ with the vibrational contribution.

In the liquid state, the atomic-level stress energies closely follow an $(1/4)k_bT$ temperature dependence. Absence of any U_o in this dependence suggests that in the liquid state, there is no "frozen in" structural contribution. This observation suggests that in the liquid state, it may not be possible to separate structural and vibrational contributions to the atomic-level stress energies.

The results of our calculations in this paper can be summarized as follows. If the long-wavelength approximation (*lwa*) is not assumed, then the pressure and shear-stress energies obtained within the considered model are approximately eight and three times smaller than $(1/4)k_bT$, respectively. If the *lwa* is assumed, then the pressure stress energy is two times smaller than $(1/4)k_bT$, while the shear-stress energy is approximately equal to $(1/4)k_bT$. In the framework of the studied model, the average atomic-level stress energies in the *lwa* are similar to those in Ref. [38].

In our present calculations of the atomic-level stress energies, it has been assumed that every atom interacts with N_c neighbors. In particular, it has been assumed that N_c is the same for every atom. Thus the situation with the nearest neighbors in the model discussed in this paper is different from the situation in MD simulations. In our model, all atoms have the same coordination number, while in MD simulations the coordination numbers of different atoms can be different.

Formulas (38) and (41) show that the average squares of the atomic-level stresses are proportional to N_c, while (37) shows that the elastic constants are also proportional to N_c. From this perspective, if all atoms have the same coordination, the atomic-level stress energies, which are proportional to the ratio of the average squares of the stresses to the relevant elastic constants, should not exhibit a dependence on N_c. However, in MD simulations, the average squares of the stresses and the average values of the elastic constants have been obtained by averaging over the atoms with different N_c. Thus a (large) part of the average atomic-level stress energies obtained in MD simulations might be related to the variations in the coordination numbers between the different atoms.

Atomic-level stresses originally have been applied to a model of metallic glass in order to describe structural disorder at $T = 0$ K [49]. Later, it was briefly discussed that it might be possible to speak about structural and vibrational contributions to the atomic-level stresses [38]. However, previously, there were no systematic attempts to separate structural and vibrational contributions to the atomic-level stresses.

Note that the rates of increase of the atomic-level stress energies in the glass state obtained from MD simulations, i.e., $(1/10)k_bT$, are still larger than the values that have been derived in this paper [see formulas (38) and (48)]. Note also that according to the present paper, the rates of increase of the pressure and shear energies should be different. However, the results from MD simulations show similar rates. This can reflect the fact that vibrations in disordered media are not plane waves as we assumed here. It also can reflect the fact that the degree of the structural disorder can also change in the glass state. For example, as temperature increases (still in the glass state), there is a weak change in the number of atoms with a given coordination as can be seen in Fig. 2 of Ref. [41]. However, this weak change can also be a consequence of the vibrational dynamics.

In the context of the considerations in this section, it makes sense to draw an analogy with the Einstein and Debye models for heat capacity. Both of these models lead to the same value of the average atomic potential energy in the classical limit of high temperatures, i.e., to $(3/2)k_bT$. The Einstein model assumes absence of any correlations between the different atoms. The Debye model, in contrast, assumes that atomic dynamics is cooperative. The assumption that the atoms with their nearest-neighbor shells act as independent harmonic oscillators is equivalent to an adoption of the Einstein model. This model describes the behavior of the atomic-level stress energies in some model liquids surprisingly well [38–40]. However, it is impossible to explain in the framework of this Einstein-like model, the nonlocal behavior of the *sscf* observed in Refs. [8,9]. In this paper, we tried to assess the nonlocal nature of the *sscf* using the Debye-like model. These considerations bring a certain degree of qualitative understanding into the data observed in Refs. [8,9]. However, the model does not describe well the dependence of the atomic-level stress energies on temperature.

Finally, we note that in the glass state, the total potential energy of the system per atom follows the $(3/2)k_bT$ law (see Fig. 3 of Ref. [41]). Thus, in the glass state, the total potential energy grows faster than the energy of the atomic level stresses, i.e., $\approx 6(1/10)k_bT$. In the liquid state, the total potential energy follows the Rosenfeld-Tarazona law $U = U_g + bT^{3/5}$ (see Fig. 3 of Ref. [41]) [50,51]. The value of the coefficient b is such that at all reasonable temperatures the total potential energy of a liquid again grows faster than the energy of the atomic-level stresses, i.e., $(3/2)k_bT$. This suggests that the energies of the atomic-level stresses do not reflect all processes that happen in the model liquid upon heating.

V. CONCLUSION

The primary goal of this paper has been to gain insights into the connection between the atomic-level vibrational dynamics and the atomic-level Green-Kubo stress correlation function. It is necessary to understand this connection in order to interpret the results of the previous MD simulations of a model liquid [8,9]. For this purpose, we considered a simple model in which vibrations are plane waves. Such representation of vibrations does not imply that we think that vibrations in liquids or glasses are plane waves. The situation in disordered materials is much more complex [26,28–30]. However, the

model that we consider is solvable, and it provides the needed insight. It also provides a recipe for the analysis in Fourier space of the atomic-level stress correlation functions obtained in MD simulations [37].

Atoms, as they move, do not decompose their motions into the orthogonal vibrational modes. Instead, they experience forces and stresses. From this perspective, the comparisons of the atomic level stress correlation functions from different liquids and temperatures may provide valuable and, probably, more physical insights into the atomic scale dynamics than considerations of the vibrational eigenmodes.

By analogy with the atomic-level stress correlation function, we addressed the possibility for the atomic scale studies of the transverse current correlation function. The energies of the atomic-level stresses also has been considered. The atomic-level stress energies obtained in the framework of the studied model are significantly smaller than the atomic-level stress energies obtained in MD simulations previously. This difference, most probably, is largely caused by the variations in the coordination numbers between the different atoms in MD simulations of glasses and liquids. In the data obtained from MD simulations, a coordination number is embedded into the definition of the atomic-level stresses. Thus it is likely that a large part of the atomic-level stress energies obtained from MD simulations is caused by the variations in coordination numbers between the different atoms. In the framework of the model studied in this paper, the coordination numbers of all atoms are the same. This is likely to be the reason for the smaller values of the energies of the atomic-level stresses obtained in this paper. Analysis of the MD data suggests that in the glass state, it might be possible to separate vibrational contributions to the atomic-level stress energies from the contribution associated with variations in coordination numbers. In the liquid state, it may not be possible to make such separation. The role of the coordination number in formation of the atomic-level stress energies deserves a more detailed investigation. Analysis of the previous MD data also shows that the rate of increase of the atomic-level stress energies is always smaller than the rate of increase of the total potential energy. This observation suggests that atomic-level stress energies do not reflect all processes that happen in the model glasses and liquids upon heating.

We demonstrated that in the framework of the model, the increase in the widths of peaks in the pair distribution function (by 40%) with the increase of distance occurs primarily because of the transverse waves. The contribution to the peaks' widths from longitudinal waves does not exhibit significant distance dependence.

ACKNOWLEDGMENTS

We would like to thank T. Egami, V.N. Novikov, and K.A. Lokshin for useful discussions.

[1] J. P. Hansen and I. R. McDonald, *Theory of Simple Liquids*, 3rd ed. (Academic Press, London, 2006).
[2] D. J. Evans and G. P. Morriss, *Non-Equilibrium Statistical Mechanics of Liquids* (Academic Press, London, 1990).
[3] J. P. Boon and S. Yip, *Molecular Hydrodynamics* (Dover, New York, 1990).
[4] *Dynamical Heterogeneities in Glasses, Colloids and Granular Materials*, edited by L. Berthier, G. Biroli, J.-P. Bouchaud, L. Cipelletti, and W. van Saarloos (Oxford University Press, 2011).
[5] L. Berthier and G. Biroli, Rev. Mod. Phys. **83**, 587 (2011).
[6] A. Furukawa and H. Tanaka, Phys. Rev. Lett. **103**, 135703 (2009).
[7] A. Furukawa and H. Tanaka, Phys. Rev. E **84**, 061503 (2011).
[8] V. A. Levashov, J. R. Morris, and T. Egami, Phys. Rev. Lett. **106**, 115703 (2011).
[9] V. A. Levashov, J. R. Morris, and T. Egami, J. Chem. Phys. **138**, 044507 (2013).
[10] T. Iwashita, D. M. Nicholson, and T. Egami, Phys. Rev. Lett. **110**, 205504 (2013).
[11] U. Buchenau, J. Chem. Phys. **134**, 224501 (2011).
[12] M. S. Green, J. Chem. Phys. **22**, 398 (1954).
[13] R. Kubo, J. Phys. Soc. Jpn. **12**, 570 (1957).
[14] E. Helfand, Phys. Rev. **119**, 1 (1960).
[15] D. J. Evans, Phys. Rev. A **23**, 2622 (1981).
[16] C. Hoheisel and R. Vogelsang, Comp. Phys. Rep. **8**, 1 (1988).
[17] S. Sharma, L. V. Woodcock, J. Chem. Soc.-Faraday Trans. **87**, 2023 (1991).
[18] L. V. Woodcock, AICHE J. **52**, 438 (2006).
[19] Hubert Stassen and William A. Steele, J. Chem. Phys. **102**, 932 (1995).
[20] Hubert Stassen and William A. Steele, J. Chem. Phys. **102**, 8533 (1995).
[21] H. Shintani and H. Tanaka, Nat. Mater. **7**, 870 (2008).
[22] H. Mizuno and R. Yamamoto, Phys. Rev. Lett. **110**, 095901 (2013).
[23] R. D. Mountain, Phys. Rev. A **26**, 2859 (1982).
[24] F. H. Stillinger and P. G. Debenedetti, Annu. Rev. Condens. Matter Phys. **4**, 263 (2013).
[25] A. Heuer, J. Phys.: Condens Matter **20**, 373101 (2008).
[26] T. Keyes, J. Phys. Chem. A **101**, 2921 (1997).
[27] R. Zwanzig and R. D. Mountain, J. Chem. Phys. **43**, 4464 (1965).
[28] S. N. Taraskin and S. R. Elliott, Phys. Rev. B **61**, 12017 (2000).
[29] N. Taraskin and S. R. Elliott, Physica B **316-317**, 81 (2002).
[30] W. Schirmacher, G. Ruocco, and T. Scopigno, Phys. Rev. Lett. **98**, 025501 (2007).
[31] A. S. Keys, L. O. Hedges, J. P. Garrahan, S. C. Glotzer, and D. Chandler, Phys. Rev. X. **1**, 021013 (2011).
[32] G. A. Appignanesi, J. A. Rodriguez Fris, R. A. Montani, and W. Kob, Phys. Rev. Lett. **96**, 057801 (2006).
[33] J. I. Frenkel, *Kinetic Theory of Liquids*, edited by R. H. Fowler, P. L. Kapitza, and N. F. Mott, (Oxford University Press, 1947)
[34] K. Trachenko and V. V. Brazhkin, J. Phys.: Condens. Matter **21**, 425104 (2009).
[35] D. Bolmatov, V. V. Brazhkin, and K. Trachenko, Sci. Rep. **2**, 241 (2012).
[36] D. Bolmatov, V. V. Brazhkin, and K. Trachenko, Nat. Commun. **4**, 2331 (2013).

[37] V. A. Levashov, J. Chem. Phys. **141**, 124502 (2014).
[38] T. Egami and D. Srolovitz, J. Phys. F: Met. Phys. **12**, 2141 (1982). See, in particular, Sec. 7 on p. 2155.
[39] S. P. Chen, T. Egami, and V. Vitek, Phys. Rev. B **37**, 2440 (1988).
[40] V. A. Levashov, T. Egami, R. S. Aga, and J. R. Morris, Phys. Rev. B **78**, 064205 (2008).
[41] V. A. Levashov, T. Egami, R. S. Aga, and J. R. Morris, Phys. Rev. E **78**, 041202 (2008).
[42] T. Egami and S. J. L. Billinge, *Underneath the Bragg Peaks: Structural Analysis of Complex Materials*, Pergamon Materials Series, 2nd ed. (Pergamon, 2012).
[43] J. S. Chung and M. F. Thorpe, Phys. Rev. B **55**, 1545 (1997).
[44] J. S. Chung and M. F. Thorpe, Phys. Rev. B **59**, 4807 (1999).
[45] M. F. Thorpe, V. A. Levashov, M. Lei, and S. J. L. Billinge, *From Semiconductors to Protein*, edited by S. J. L. Billinge and M. F. Thorpe (Kluwer Academic/Plenum Publishers, New York, 2002).
[46] MAPLE (5). Maplesoft, a division of Waterloo Maple Inc., Waterloo, Ontario.
[47] For transverse waves, it is convenient to represent $\hat{\boldsymbol{e}}_{\boldsymbol{q}}^{T}$ as a linear combination of vectors $\hat{\boldsymbol{e}}_{\boldsymbol{q}}^{1}$, $\hat{\boldsymbol{e}}_{\boldsymbol{q}}^{2}$, which are orthogonal to $\hat{\boldsymbol{q}}$ and to each other. If angles θ and ϕ define the direction of $\boldsymbol{q}$, then we can chose $\hat{\boldsymbol{e}}_{\boldsymbol{q}}^{1} \equiv [\cos(\theta)\cos(\phi), \cos(\theta)\sin(\phi), -\sin(\theta)]$ and $\hat{\boldsymbol{e}}_{\boldsymbol{q}}^{2} \equiv [\hat{\boldsymbol{q}} \times \hat{\boldsymbol{e}}_{\boldsymbol{q}}^{1}] = [-\sin(\phi), \cos(\phi), 0]$. Thus we write $\hat{\boldsymbol{e}}_{\boldsymbol{q}}^{T} \equiv \hat{\boldsymbol{e}}_{\boldsymbol{q}}^{1}\cos(\psi) + \hat{\boldsymbol{e}}_{\boldsymbol{q}}^{2}\sin(\psi)$. In (43), after taking the square, averaging should be done over ψ and then over the directions of $\hat{\boldsymbol{q}}$. For longitudinal waves, $\hat{\boldsymbol{e}}_{\boldsymbol{q}}^{L} || \hat{\boldsymbol{q}}$.
[48] L. D. Landau and E. M. Lifshitz, *Fluid Mechanics*, 2nd ed. (Reed Educational and Professional Publishing, London, 1987).
[49] T. Egami, K. Maeda, and V. Vitek, Phil. Mag. A **41**, 883 (1980).
[50] Y. Rosenfeld and P. Tarazona, Mol. Phys. **95**, 141 (1998).
[51] Y. Gebremichael *et al.*, J. Phys. Chem. B **109**, 15068 (2005).